The Thesis Committee for Joseph Michael Nissen
Certifies that this is the approved version of the following thesis:

Methodology for Determining Design Rules for Helical Channels in Glass Components Produced via Selective Laser Sintering

APPROVED BY
SUPERVISING COMMITTEE:

Supervisor: _____
Desiderio Kovar

Co-Supervisor: _____
Joseph J. Beaman, Jr.

Methodology for Determining Design Rules for Helical Channels in Glass Components Produced via Selective Laser Sintering

by

Joseph Michael Nissen

Thesis

Presented to the Faculty of the Graduate School of

The University of Texas at Austin

in Partial Fulfillment

of the Requirements

for the Degree of

Master of Science in Engineering

The University of Texas at Austin

May 2020

Dedication

I'd like to first dedicate this work to my mother, my father, and my sister for being the best family I could've asked for. Your love and support over the years has been pivotal in allowing me to pursue my goals, and I wouldn't trade it for anything.

Additionally, I'd like to dedicate this work to my girlfriend, Maggie, for always pushing me to be the best version of myself. Your drive and motivation in your own work has truly been inspiring to witness, and I have you to thank for being by my side throughout this journey.

Finally, I would be remiss if I didn't mention my friends, both new and old, for being the most wonderful support network. Without those relationships to fall back on, I don't know that I would've been able make it to this point. Thank you all, from the bottom of my heart.

Acknowledgements

Financial support for this work was provided by L3Harris Technologies. Additional support from Douglas Sassaman, Scott Snarr, Tim Phillips, and Patrick Snarr across all aspects of experimentation was critical towards the completion of this research. I'd like to personally thank Dr. Joseph Beaman and Dr. Desiderio Kovar, as this research would not have been possible without their constant guidance, expertise, and support.

Abstract

Methodology for Determining Design Rules for Helical Channels in Glass Components Produced via Selective Laser Sintering

Joseph Michael Nissen, M.S.E.

The University of Texas at Austin, 2020

Supervisor: Desiderio Kovar

Co-supervisor: Joseph Beaman

The accuracy of geometric features is one of the main hurdles in advancing the use of additive manufacturing for the production of functional parts. Much research has gone into quantifying the dimensional accuracy and design limitations of various types of additive manufacturing utilizing a wide variety of materials and manufacturing techniques. Design rules can be found for parts produced using selective laser sintering for polymers with features such as thin walls and through-holes. However, these rules have not been studied for more complex features such as helical channels produced from glass or ceramic materials. In this study, we propose a methodology for predicting the success and failure in accurately reproducing internal helical channels produced via selective laser sintering. Parameters that define these geometries include the channel diameter and length and the helix diameter and pitch. The methodology is experimentally validated for parts created

via indirect selective laser sintering from mixtures of glass and nylon powders. Feature resolution is quantified for successful production of both green parts as well as the final parts after debinding and sintering. This methodology is demonstrated for the production of glass components that are designed to manipulate light via the addition of orbital angular momentum in order to add an optical degree of freedom to the system.

Table of Contents

List of Tables

List of Figures

Chapter 1: Introduction

The production of glass components for optical applications often requires complex geometrical features and small batch sizes in order to suit a part to its use-case. Production of these parts has historically been handled using a variety of methods including machining, injection molding, and in some cases, additive manufacturing. Each of these methods have benefits and limitations making them suitable for some applications and less applicable for others. For example, machining, a subtractive manufacturing method in which material is removed from an initial form, is widespread, accurate and precise, and suitable across a wide range of materials. It also lends itself well to the production of small batch sizes, as the cost scales relatively linearly with the number of parts produced. However, it is inherently limited regarding the geometries it can achieve. Any internal features need to be accessible by a cutting tool, which imposes limits that restricts the fabrication of many features, specifically those that are not simply straight through-holes. Injection moldering allows for the production of more complex geometries for glass parts compared to machining, but the tooling cost associated with production is quite high. For this reason, it is not amenable to small batch sizes due to the large upfront cost. There are also inherent geometry limitations due to the complexity of the molds and the process in which the material is introduced to produce the parts. More recently, additive manufacturing has proven to be a viable option for producing complex glass parts. Additive manufacturing, which builds components layer-by-layer using a material feedstock, can produce complex geometries that other traditional manufacturing methods cannot. Further, it is amenable to small batch sizes because there is no need for part-specific tooling beyond the machine being used to fabricate the parts.

Several methods of additive manufacturing have been employed to produce complex glass components. Fused deposition modeling (FDM) utilizing a molten glass feedstock has produced optically transparent glass (Klein *et al.* [1]). FDM is a nozzle-based approach where material is heated just beyond the melting point such that it can viscously flow. The nozzle and/or print bed moves according to the shape of the component being produced which deposits a stream of molten material. Since this material is only slightly above the melting point, it quickly hardens allowing it to maintain the desired geometry. The main drawback of this approach is the necessity for supports for complex geometries such as overhangs. These supports must be removed which limits the scale in which the parts can be fabricated.

Stereolithography has also been employed to produce complex ceramic shapes (Zocca *et al.* [2]). This process involves photopolymerizing a resin which contains the desired ceramic feedstock. An ultraviolet light source cures the part layer by layer which is supported within a vat of resin. This process can produce very accurate and precise geometries but suffers a similar drawback to FDM in the sense that it requires support structures for complex geometries which limits its application for optical-quality parts. Additionally, the non-ceramic material must be removed to form the final part.

Selective laser sintering (SLS) is another option that has been successfully employed in the creation of complex glass parts. This process utilizes a laser, a powder feed system, and a heated powder bed and build chamber to produce geometrically complex, three-dimensional parts. One benefit of selective laser sintering over the previously mentioned methods is that the powder bed supports the parts during construction. Since the part is being built within the powder bed, there are never any

unsupported geometries, vastly increasing the possibilities for feature generation. Similar to creating ceramic parts with stereolithography, this process utilizes a polymer material to bond the structure together which must be removed later. Despite this, the geometrical benefits make this a suitable method for this research.

In order to produce parts via SLS, a slicing program takes an imported CAD model and transforms it into two-dimensional layers that are approximately 100 μm thick. A powder feed system spreads a uniform layer of powder onto a preheated powder bed using a counter-rotating roller. After powder deposition, the laser precisely scans the powder bed utilizing a pair of galvanometers according to the two-dimensional model created by the slicer. The combination of preheating and the laser is used to bring the powder slightly above the melting point, allowing it to selectively bond to surrounding particles as well as to the powder layer below it. Following scanning of each layer, the piston supporting the power bed is lowered by an amount equal to the layer height, another layer of powder is spread, and the process is repeated until the construction of the part or parts is complete. A schematic of SLS is shown in Figure 1.

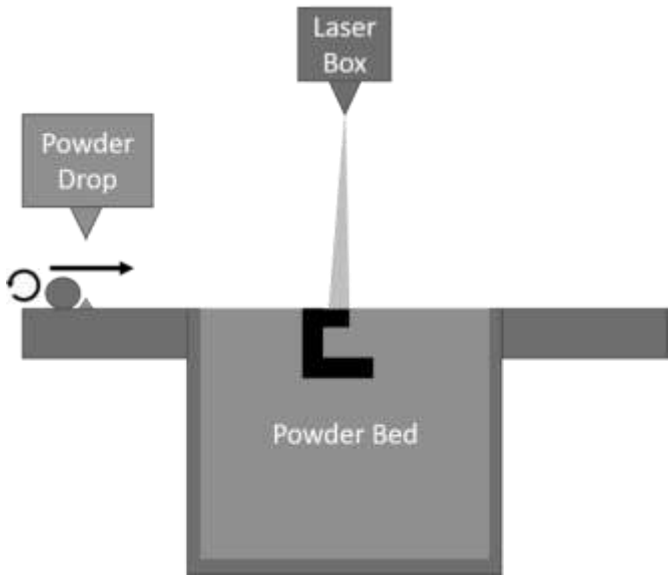

Figure 1. Selective Laser Sintering Schematic

Selective laser sintering has been used extensively in industry due to several benefits inherent to the process that may not be achieved utilizing other manufacturing methods. SLS allows for the creation of complex geometries that may not be possible utilizing traditional manufacturing methods. By utilizing a layer-by-layer approach, internal features and geometries can be created that otherwise could not be. Additionally, powder-bed fusion additive manufacturing methods such as SLS do not require support structures that may be required with other AM methods such as fused deposition modeling or stereolithography due to the inherent support from the powder bed throughout the manufacturing process.

Polymers such as nylon 11 and 12 are often used for *direct* selective laser sintering, due to their relatively large thermal processing windows and relatively low melting temperatures. Design rules have been studied extensively to provide guidelines to

successfully resolve features for parts made with this process. Examples of design guidelines for SLS can be seen in work by Allison *et al.* [3]-[5] and Adam and Zimmer [6]. Studies have also been done to validate the strength (Milisits [7]), roughness (Thompson [8]), and porosity (Deckers *et al.* [9]) of parts produced in this manner to drive design for end-use parts. Research in this field has focused on simple geometries and features such as wall thickness, bore diameter and depth, and minimum resolvable feature size.

Despite success with polymers, the production of ceramic and glass parts in a similar fashion has historically been difficult. This is due the low resistance to thermal shock that ceramics and glasses have as well as their high melting temperatures, which makes preheating and laser melting more difficult. These challenges have been overcome by utilizing *indirect* selective laser sintering, which utilizes a mixture of ceramic or glass powder and polymer powder. For indirect SLS, mixed powder is used with laser processing parameters based on those of the polymer. The result is a "green part" in which the ceramic/glass particles are bound together by the resolidified polymer. The presence of the polymer introduces the need for debinding (the process of removing the polymer binder) and densification via sintering at a higher temperature to produce the final ceramic/glass part. Although the shrinkage that accompanies densification complicates part design, indirect SLS allows for the production of ceramic and glass parts with complex geometries which may not be feasible with other manufacturing techniques.

The additional processing steps of debinding and sintering also affect factors such as final density and feature resolution when compared to standard polymer SLS parts. General design guidelines used for parts made via SLS often work satisfactorily with indirect SLS and there are many examples of complex ceramic parts being produced

utilizing indirect SLS (Xiao *et al.* [10], Shahzad *et al.* [11]). However, there is no current methodology that can be used to define the capabilities and limitations of complex geometric features produced via indirect SLS.

One example where glass parts with complex geometries would be desirable is in photonic applications where light is manipulated precisely using controlled geometries. Given a predictable reflectivity response, it may be possible to add orbital angular momentum to light waves through the use of an additively manufactured glass cylinder containing a helical internal channel. This offers extraordinary potential benefits in terms of information transfer and quantum computing by increasing the bandwidth a beam of light can feasibly carry (Wang *et al.* [12]). This increase in bandwidth is associated with an increase in the quantum number of the photons. Applying orbital angular momentum to light beams represents a theoretically limitless increase in this potential bandwidth because the states that the quantum number can take are themselves theoretically limitless (Zhao *et al.* [13]). Utilizing a glass cylinder with a helical channel to achieve this could be used as a fiber optic cable preform specifically to add orbital angular momentum to the light traveling through the individual fibers making up the cable.

Fiber optic cables are traditionally manufactured through a process involving the creation of a preform which is drawn to great lengths to reduce the cross-sectional area to form the final fiber (Keck & Schultz [14]). Commonly in this process, glass tubes are injected with a gas mixture composing of materials such as silicon tetrafluoride and germanium tetrachloride which is determined by the desired refractive index of the final glass. This procedure is referred to as Modified Chemical Vapor Deposition (MCVD). This

causes soot builds up on the interior surface of the tube which is heated further to form a solid glass layer (Yeh [15]) A depiction of this can be seen in Fig. 2.

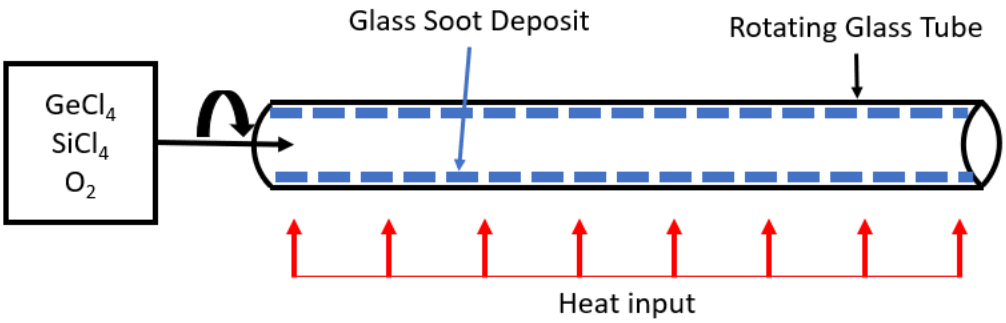

Figure 2. Simplified MCVD Process for soot deposition for optical fiber production

A further addition of heat causes the glass tube to collapse on itself forming a solid cross section. This "preform" can then be drawn using a drawing tower to form fibers hundreds of meters long. The diameter of the resultant fiber can be controlled and maintained by accurately controlling the tension applied in the drawing process.

More recently, methods have been implemented to increase the bandwidth of fiber optic cables by changing the way in which they are produced to introduce orbital angular momentum. Spiral phase plates have been used to achieve this utilizing a transparent form with refractive index n whose thickness increases around the central axis of the plate (Massari *et al.* [16]). This adds a phase delay to the light beam allowing for the generation of orbital angular momentum. While this has produced successful results, fabrication is complicated and generally expensive due to the nature of the required geometry (Beijersbergen *et al.* [17]).

Another method involves producing a preform with multiple channels arranged cross-sectionally in a hexagon. This preform is then twisted as it is drawn to produce an array of helical channels running throughout the part. This has been shown to produce orbital angular momentum within the fiber optic cable (Russell *et al.* [18]). However, it is not without limitations. Twisting the entire preform introduces geometric inaccuracies which scale with the radial distance from the center of the preform itself. They also introduces stresses and strains within the part which influence the optical performance. These inaccuracies provide practical limitations to the theoretical boundlessness that this technology can provide. Producing robust parts with minimal geometric inaccuracies may represent another opportunity to produce orbital angular momentum in fiber optic cables.

An additive manufacturing approach allows the complex features necessary to produce such a part that are not possible using traditional manufacturing methods. This research is aimed at quantifying design limitations as they pertain to internal helical channels in ceramic parts produced via indirect SLS and to establish design rules to predict successful feature resolution following indirect SLS, debinding, and densification via sintering. This research methodology can be extended to any powder mixture suitable for the SLS process and can be used in tandem with previously established design rules to further the potential of complex parts created in this manner. Further, this methodology is used to design and fabricate parts that may suitably apply orbital angular momentum to light through fiber optic cables in order to maximize bandwidth in optical systems by implementing an additional optical degree of freedom.

Chapter 2: Methodology for Determining Design Rules for Helical Channels in Glass Components Produced by Selective Laser Sintering

2.1: Materials and Methods

The materials used were 3124-2 glass frit (Ferro, USA) and Polyamide 650 (Advanced Laser Materials, USA). The glass is a leadless, high calcium, borosilicate frit that is frequently used as a ceramic glaze. It has a density of 2.534g/cm^3 (Fluegel [19]) and a melting temperature of ~850°C. Observations via scanning electron microscopy confirm that the morphology is non-spherical with a mean particle size of 3-5 μm. Per the manufacturer, polyamide 650 has a mean particle size of 55 μm with a $D_{v,10}$ of 30 μm and a $D_{v,90}$ of 100 μm and a melting temperature near 180°C. This makes it an excellent candidate for SLS in general, but also as a polymer binder for indirect SLS. Fig. 3 shows the methodology for producing glass parts as well as the steps utilized to create the powder mixture itself.

Note: Content from this chapter pulled in part from "Methodology for Determining Design Rules for Helical Channels in Glass Components Produced via Selective Laser Sintering" by Joseph Nissen, Desiderio Kovar, Joseph Beaman, Susanne M. Lee, and Joseph A. Desjardins, Additive Manufacturing, in preparation, 2020

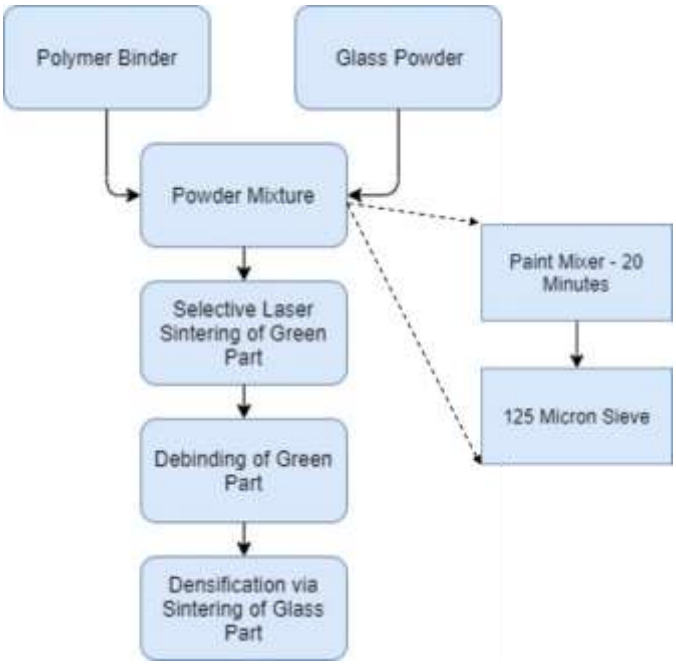

Figure 3. Flow chart for preparation of glass samples via indirect SLS

The feedstock powders were produced by mixing powders at percentages of 48.6 vol% polymer and 51.4 vol% glass for a total mass of 1.5 kg. The powder mixture was then blended in a 3.8 liter can utilizing a mechanical paint mixer (Speed Demon SQ, Red Devil Equipment Co, Plymouth, Minnesota) for five cycles that each had a duration of four minutes. Between each mixing cycle, the contents of the container were shaken to loosen any powder from the sides of the can in order to promote additional mixing at each subsequent step and to reduce the likelihood of agglomerates forming. Following mixing, the powders were forced through a 125 μm sieve in order to break up agglomerates that still remained from the initial individual powders. A sieve size of 125 μm was selected to ensure all remaining powder particles were of a size suitable for SLS (125 μm approaches

the upper limit). Scanning electron micrographs of the individual powders as well as the resulting mixed powder are shown in Fig. 4.

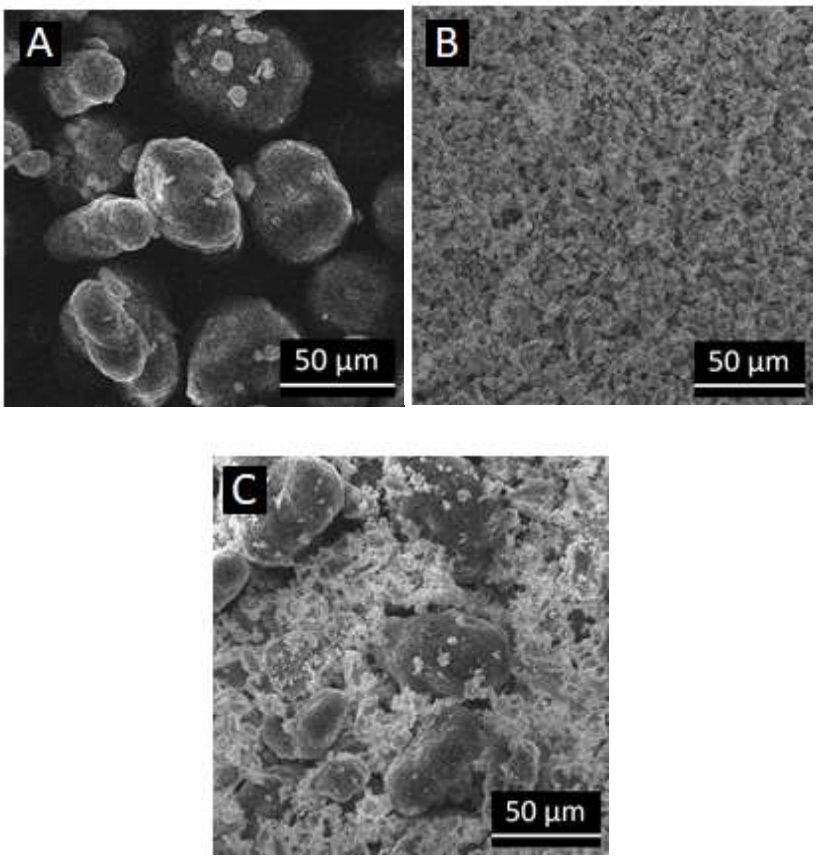

Figure 4. SEM micrographs of (A) nylon powder, (B) glass frit, (C) nylon/glass frit after mixing.

It is apparent from Fig. 4c that the mixture is somewhat heterogeneous with large particles of the nylon separated by regions that contain many glass particles. Sample bars were made to confirm that robust green parts could be produced using this powder mixture and it was found that although this morphology was not ideal, it was suitable for use as a

feedstock for SLS because the nylon was distributed evenly enough to provide an adequate melt pool to bond the glass particles together.

The SLS process for production of the parts made for this study was performed with a custom-built SLS system utilizing a CO_2 laser at a wavelength of 10.6 μm, a preheated powder bed, and a nitrogen atmosphere. The processing parameters that were used are presented in Table 1.

Parameter	**Value**
Preheat Temperature	181°C
Laser Power (for fill)	6.08 W
Laser Power (for outline)	4.29 W
Scanning Speed (v)	1000 mm/s
Scan Line Overlap (φ)	52.1%
Beam Diameter (b)	0.4 mm

Table 1. Processing parameters used for indirect SLS of polymer/glass parts

The processing parameters were selected to diminish defects (curling, shifting, etc.) that occurred during printing as a result of the addition of the glass powder. Total energy density is given by

$$E = \frac{W}{(1-\varphi)\cdot b\cdot v} \qquad \text{(Eq. 1)}$$

where E = energy density, W = laser powder, b = beam diameter, and v = scan speed. For the values of laser power, beam diameter and scan speed that were used to produce the nylon/glass parts for this study, the energy density was 0.032 J/mm^2.

Following the shape formation of the green parts via SLS, debinding was performed to remove the polymer binder. Debinding was performed by slowly heating the part through its critical temperature range in order to allow the polymer to pyrolize at a slow enough rate to not cause distortion or cracking of the part. The parts were buried in silica powder within an alumina crucible and placed in a tube furnace. The silica powder had a higher melting temperature than the glass frit, so it served to insulate the part from the alumina crucible while also preventing chemical reactions with the crucible. Air was flowed through the tube furnace at 0.13 liters/minute to carry away the decomposition products. The alumina crucible was covered to ensure that this airflow produced minimal convective cooling to reduce the risk of warping of the sample.

In order to establish a debinding temperature profile, thermogravimetric analysis was done of the powder mixture. The results of this can be seen in Fig. 5. The critical temperature range indicated on the TGA plot between the red bars is the critical temperature range in which the polymer binder begins to off-gas. Any reduction in mass

before this point is primarily moisture loss. Once the temperature gets above the upper limit of this range, there has been enough polymer removed that there is sufficient open porosity to allow the final remaining nylon to off-gas. It is important to ramp the temperature up slowly within the critical temperature range in order to mitigate the risk of bloating or cracking. This occurs if the binder heats and expands too quickly before it's able to diffuse through the microcracks in the part.

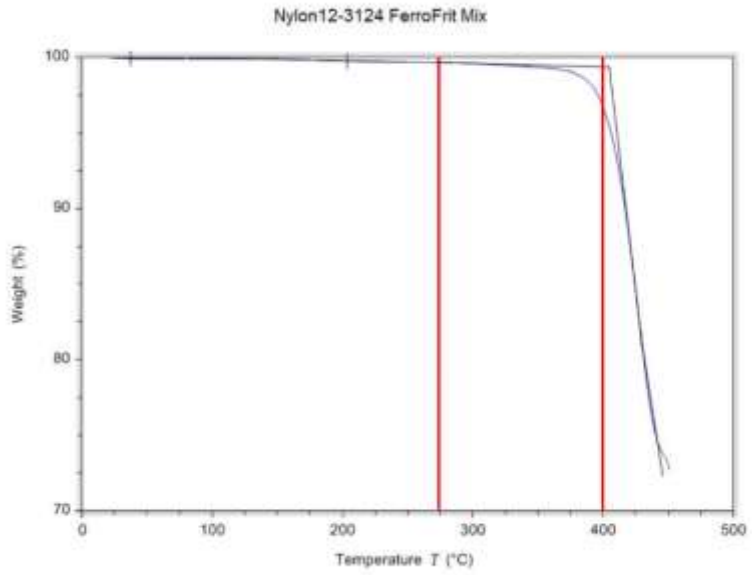

Figure 5: Thermogravimetric Analysis of the Powder Mixture

The resultant temperature profile for debinding and carbon removal is shown in Fig. 6. The initial ramp rate was 60˚C/min to 275˚C but the ramp was paused at 148°C and the temperature was then held at this temperature for 2 hours. The ramp rate through the critical temperature region of 275-400°C was slowed to 2°C/hr. Above 400˚C, the ramp

rate was increased to 4°C/hr, 6°C/hr, and finally to 60°C/hr to a maximum temperature of 500˚C. Following binder removal, the temperature was increased further to remove any carbon deposits remaining in the part following pyrolysis. The result after this heat treatment was a porous, glass part.

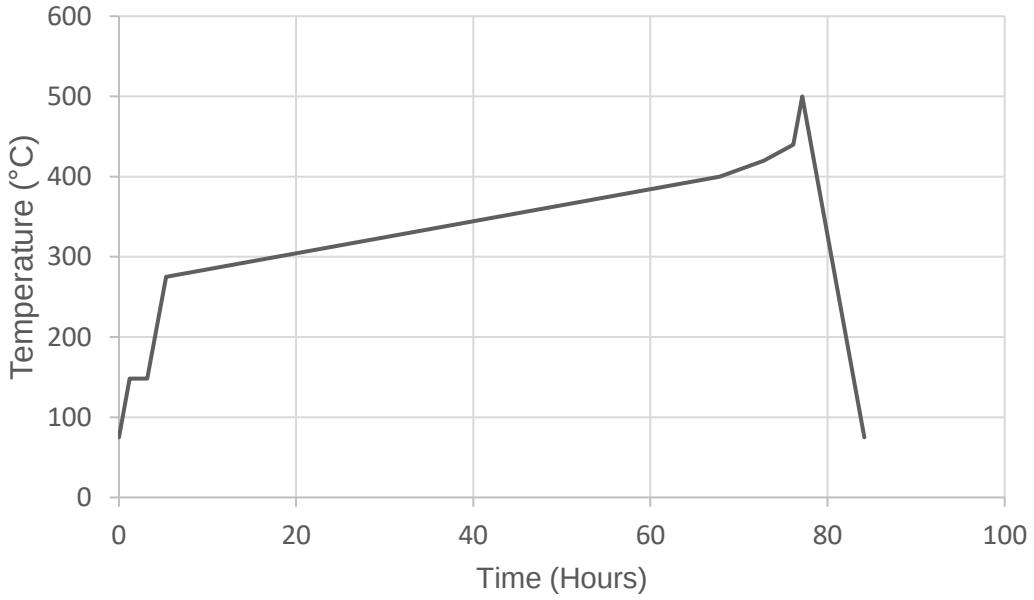

Figure 6. Temperature profile for debinding

Following the debinding and carbon removal steps, the parts were sintered to bond the particles and reduce porosity. After debinding, the parts were very fragile. For this reason, the crucible was not moved within the tube furnace after the debinding step. Rather, the air flow was stopped and the heating profile for sintering was then started. To select the sintering temperature for glass parts containing complex features, it was necessary to

balance two competing phenomena: the sintering temperature must be high enough to allow the glass to flow at the microscopic scale so that voids left from the removal of the binder and between glass particles can be filled, but not so high that the flow alters the macroscopic geometry of the part. Simple, flat bars were sintered at various temperatures in order to identify the highest temperature that did not result in slumping. Results from this can be seen in Table 2.

Temperature	**Slumping**
570°C	No
580°C	Yes
590°C	Yes
600°C	Yes

Table 2. Sintering temperature and the qualitative presence of slumping following sintering.

Based on these results, it was determined that a sintering temperature of 575˚C met the necessary criteria to maximize density while minimizing the risk of slumping. A heating and cooling rate of 60˚C/hr with a 1 hour hold at the sintering temperature was used for the sintering treatment. After sintering, the parts were removed from the tube furnace and the density was measured. Water permeation suggested that the sintered samples contained residual open porosity and thus the Archimedes method could not be used to measure the densities of the samples. To obtain densities, the cross-sections were

analyzed at 10 points along the lengths of the samples using x-ray tomograph slices. The pore channel areas were subtracted from the overall cross-sectional areas and the volume of each segment between neighboring slices was calculated by multiplying the areas by the length between slices. The overall length was then obtained from the outer dimensions of the part and the segment lengths were then scaled by overall length to obtain the overall volume of the glass regions of the samples. The mass was then divided by this overall volume to obtain the densities. The mean density ± one standard deviation obtained from the measurements from 7 samples was 1.56 ± 0.26 g/cm^3 (62% ± 10.4%).

Each part contained a helical channel, as shown in Fig. 7. The relevant parameters that define the channel are the length, channel diameter, helix diameter, and pitch. These four quantities describe all variations that a helical channel can have within this design space. Note that the outer diameter was varied as necessary to ensure that the channels were fully encased within the cylindrical outer shell.

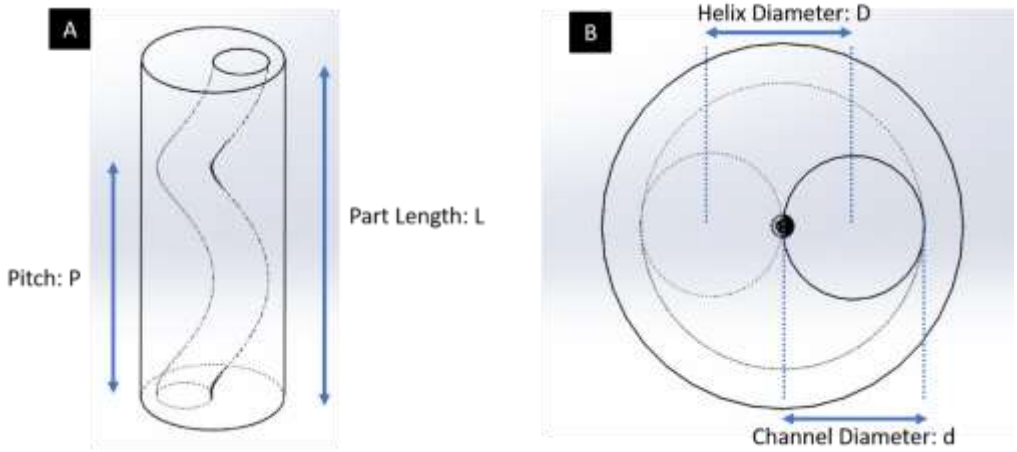

Figure 7. Dimensions for parts containing helical channels: (A) Isometric view, (B) Top view

After removing the parts from the SLS machine, they were tapped lightly with a metal rod followed by injection of compressed air into the channel at a pressure of 100 psi in order to remove the remaining loose powder from the channel. The metric of success for channel clearing for each part was determined only using a combination of percussive taps and compressed air. Although it is possible to clear stubborn channels through means such as inserting a wire into the channel, doing so can damage the structural integrity of the walls and thus only non-intrusive methods were employed in this study.

The success or failure of each part was recorded, and green parts with channels that were successfully cleared were debinded and sintered in order to produce the final ceramic parts. X-ray tomography was performed on representative sintered samples to identify any defects that occurred during the debinding and sintering steps.

2.2: Definitions of Geometrical Parameters

The variables impacting the ability to clear an internal channel for a part made through selective laser sintering are the diameter of the channel (d), the length of the part (L), the pitch of the helix (P), and the diameter of the helix (D). The ranges for each variable studied are presented in Table 3.

Variable	**Minimum**	**Maximum**
Channel Diameter (d)	0.5 mm	5 mm
Length (L)	5 mm	66.7 mm
Pitch (P)	5 mm	81 mm
Helix Diameter (D)	1 mm	6 mm

Table 3. Ranges of design variables

To reduce the four variables and consider the relationships between them, two dimensionless parameters are defined. The first, is the *scaled diameter*, σ, which is given by

$$\sigma = \frac{d}{L} \qquad \text{(Eq. 2a)}$$

where d = channel diameter and L = part length. The second is the *tortuosity*, τ, which is given by

$$\tau = \frac{p}{D} \qquad \text{(Eq. 2b)}$$

where p = channel pitch and D = helix diameter.

The physical significance of σ is that when either the diameter of the channel is increased or the channel length is decreased, σ increases and the channel becomes easier to clear of loose powder. Logically, a larger channel diameter would result in a higher likelihood of powder free flowing out of the channel. Additionally, shorter parts produce channels more likely to clear due to the reduction in friction forces along the interior walls of the channels compared to longer parts. Thus, a larger σ value increases the likelihood that the channel will be successfully cleared. The physical significance of the tortuosity is that it represents a measure of the deviation of the channel from a straight channel. For example, as the helix diameter decreases (and the channel approaches becoming a straight through-hole), τ approaches infinity. This represents an increase in the ease of channel clearing. A reduction in channel pitch results in a more tightly bound channel (thus complicating the clearing of the channel) resulting in a lower τ value. Thus, channels with a large value of τ are easier to clear of powder than those with a small τ value.

2.3: RESULTS

2.3.1: Green Parts

Initially, ten different part geometries with three samples from each geometry were built and the ability of the powder to be cleared was measured. For each of these ten geometries, the four individual dimensional parameters (channel diameter, part length, helix diameter, and pitch) of each trial were identical. Images of green parts after clearing and final parts after sintering are shown in Fig. 8.

Figure 8. Green Parts (Left). Sintered Parts (Right)

Notably, results were consistent between samples that had the same geometry; i.e. the channels in all three samples for each geometry were either successfully cleared or the channels for all three samples could not be cleared. These geometries were used to identify the critical ranges in which more trials would be necessary. Because of the consistency in the results for each geometry from the initial builds, only a single sample was produced for

each geometry for all of the subsequent builds. Note that, the same values of σ and τ can be obtained with different combinations of d, p, D, and L.

The results from the initial builds suggested that a dividing line could be defined given by

$$\sigma = -0.008(\tau) + 0.2 \qquad \text{(Eq. 3)}$$

Samples with combinations of σ and τ above this line could generally be cleared while samples with values below this line could generally not be successfully cleared. Based on these preliminary tests, additional build geometries that produced values of σ and τ that were just above and just below this line were produced to better test the validity of this approach. Notably, it was determined that there was a critical upper diameter of 4.5 mm at and above which all channels could be cleared and a critical lower diameter of 1.5 mm below which no channels could be cleared, independent of σ and τ. These points therefore define the window in which this model is applicable. Thus, parts with channel diameters of less than or equal to 1.5 mm or greater than or equal to 4.5 mm were not included in the final data set.

A plot of the σ versus τ is presented in Fig. 9. Table 5 in the appendix shows the complete data set for the 63 samples that were prepared. In the plot, open symbols represent combinations of σ and τ with successfully cleared channels, closed symbols represent combinations of σ and τ with unsuccessfully cleared channels, and the half-filled symbols represent combinations of σ and τ where the results depended not only on σ and τ, but also on which specific values of d, p, D, and L that were selected. Also included in this plot is

the linear relationship defined by eq. 3 (line). The plot shows that this linear relationship can generally be used to predict whether a channel can be cleared. For samples with combinations of σ and τ that lie above the line, 93.3% of the samples contained channels that were successfully cleared of loose powder. For samples with combinations of σ and τ that lie below the line, a failure rate of 79.2% was measured.

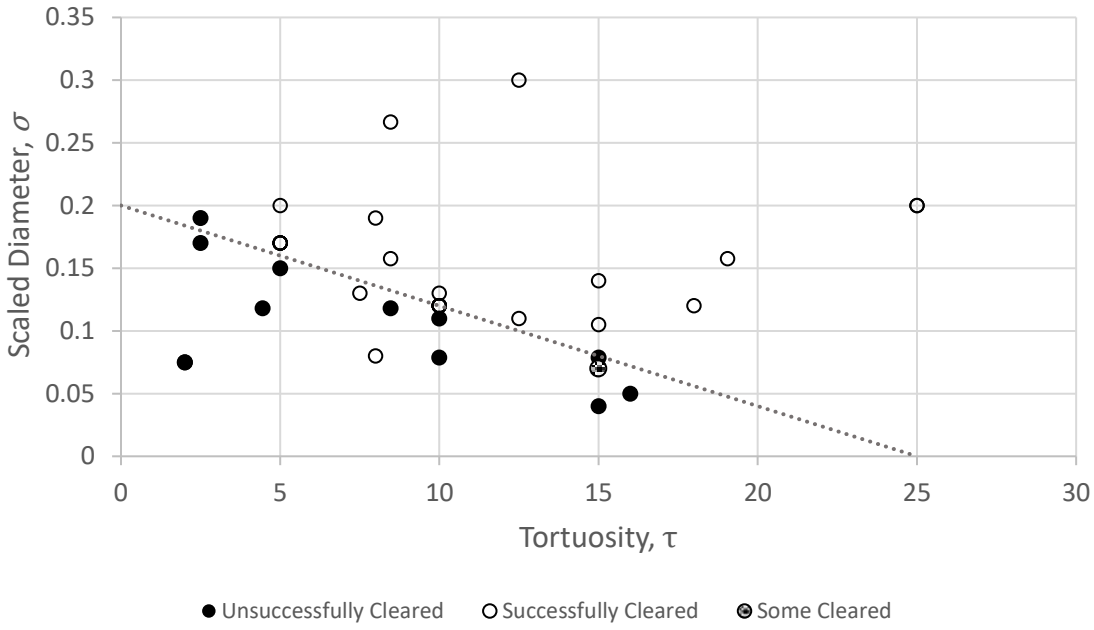

Figure 9. Scaled diameter versus tortuosity. Open symbols represent combinations of σ and τ with successfully cleared channels, closed symbols represent combinations of σ and τ with unsuccessfully cleared channels, and the half-filled symbols represent combinations of σ and τ where the results depended not only on σ and τ, but also on which specific values of d, p, D, and L that were selected**.** The line is defined by eq. 3.

2.3.2: Sintered Parts

Because sintering of glass powders requires viscous flow, it is possible that the channels that were successfully cleared in the green state could collapse during sintering and this represents a potential second failure mechanism. X-ray tomography was conducted on a representative subset of sintered parts with channels deemed most likely to close off or collapse in order to confirm that the channels stayed open during the sintering process. This also allowed for the visualization of distortion anywhere along the length of the channel that may have occurred at any stage of the process. Cross-sectional scans of the entirety of the part are taken at high magnification with a voxel resolution of approximately 11µm × 11µm × 11µm. A representative cross-sectional slice from the x-ray tomography scans is presented in Fig. 10.

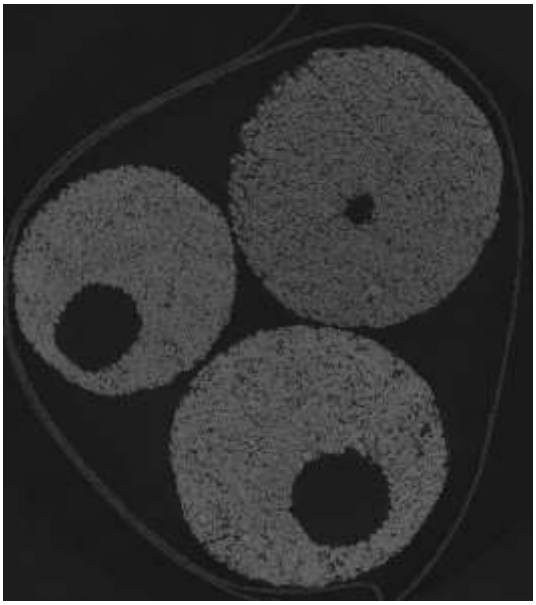

Figure 10. A slice from an x-ray tomograph showing the cross-sections from three sintered samples.

The cross-sectional dimensions of the channels were measured and the deviations from the desired geometries were quantified using ImageJ (NIH, USA) software. Circularity, roundness, and aspect ratio were determined at 10 equidistant slices taken along the length of each part utilizing the following formulas:

$$Circularity = 4\pi\left(\frac{A}{P^2}\right) \qquad \text{(Eq. 4a)}$$

$$Roundness = \frac{4A}{\pi {M_a}^2} \qquad \text{(Eq. 4b)}$$

$$Aspect\ Ratio = \frac{M_a}{M_i} \qquad \text{(Eq. 4c)}$$

where A = the cross-sectional area of the channel, p = the perimeter of the channel, M_a = major axis of the channel, and M_i = minor axis of the channel. From the equations, it is apparent that in the ideal case, the circularity, roundness, and aspect ratio are all equal to 1 and larger or smaller values represent errors in the geometry. Graphs of these values across all samples that were measured are plotted in Fig. 11.

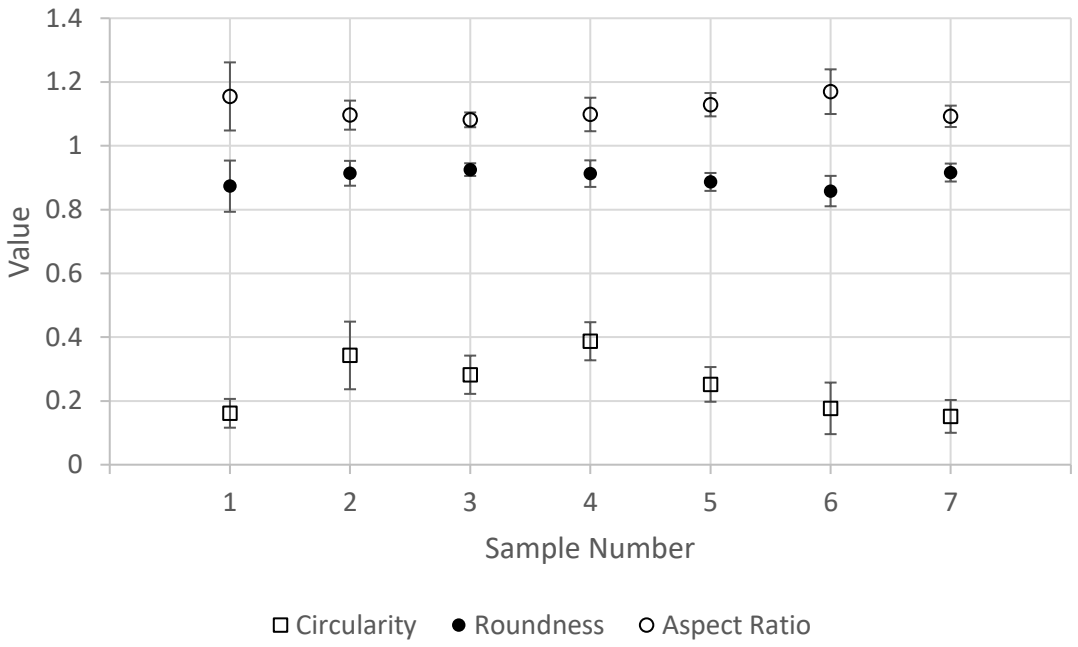

Figure 11. Average measured values of circularity, roundness, and aspect ratio

Roundness describes the ratio of the area of the circle compared to the area of a circle of diameter equal to the major axis of the channel. The average measured roundness across all samples varied from 0.86 to 0.93, with an average of 0.90 and a standard deviation of 0.05. These values are fairly close to the ideal (and maximum) value of 1.0.

The aspect ratio measures the ratio of the longest diameter to the shortest diameter. The measured aspect ratios varied from 1.08 to 1.17, with an average of 1.12 (compared to an ideal value of 1.0) and a standard deviation of 0.067. This indicates that the channels are slightly oval. This likely was a result of the choice of the build orientations that were used during the SLS of the parts; all the parts were built with the axis of the cylinder lying

in the plane of the layer. Aspect ratios closer to one could likely be achieved if the axis of the cylinder was oriented such that it was perpendicular to the plane of the layer.

Circularity is a measure of the ratio of the perimeter of a circle to the perimeter of the sample. This parameter is highly sensitive to the resolution of the images from which the parameter is calculated because samples can exhibit very low values of circularity if the resolution of the images is sufficient to capture the roughness. The measured circularity ranged from 0.16 to 0.39 with an average of 0.25 and a standard deviation of 0.11. The large deviation from one occurred because the roughness of the channel surfaces was on the order of the polymer particle size (~55 μm) and therefore was easily resolved by the tomographs.

Deviations in the diameter of the channels along the lengths of parts were also analyzed from three representative tomographs. To compare the relative errors in the channel diameter for these samples that had different geometrical parameters, the diameter for each slice, d_n, was normalized by the average diameter for that sample, d_{ave}. Fig. 12 is a plot of d_n / d_{ave} versus the slice number, n, measured from the end of the sample.

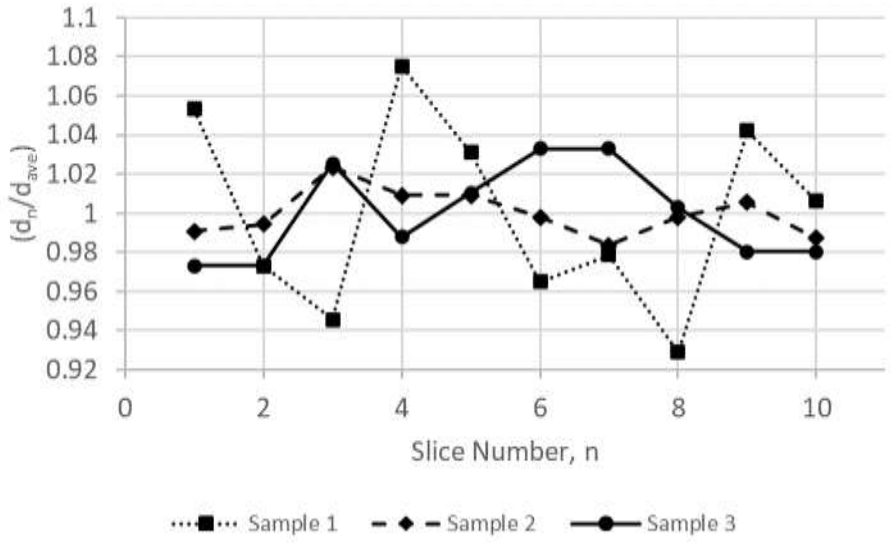

Figure 12. Normalized Channel Diameter, (dn /dave), versus the Slice Number, n for Sample 1 (d=5, p=10, D=5, and L=66.7, d/L=0.075, and p/D=2), Sample 2 (d=4, p=38.1, D=2, and L=25.4, d/L=0.157, and p/D=19.1), and Sample 3 (d=2.0, p=50, D=2, and L=10, d/L=0.200 and p/D=25). All dimensions in mm.

For all three samples, there is no observable systematic variation in the dimensions of the channel along the length of the sample. This is ideal for optical applications (as well as many others) where geometric uniformity along the length of the channel is important. In each case the channel diameter remained relatively constant with depth into the sample, but there were small variations in the channel diameter from slice to slice. These relative variations in the diameter of the channels varied from ±2% - ±7%, depending on the sample. The samples with the largest relative variation in channel diameter was sample 1 which had a similar channel diameter to the other samples, but a smaller channel pitch and much longer length. Thus, Sample 1 had the smallest d/L and p/D of the three samples that were analyzed. From this data, it is apparent that increasing d/L and p/D decreases the relative variation in the diameter of the channel. It is also important to note that the absolute

variation in the channel diameter scales with the diameter of the channel. Thus, the sample with the smallest diameter exhibited the smallest absolute variation in channel diameter.

2.4: DISCUSSION

A methodology was developed to predict whether parts with complex internal channels can be successfully produced using indirect SLS from glass powders. This methodology utilized two dimensionless parameters, the scaled diameter and the tortuosity, to describe the ease in which loose powder could be removed from the channel in the green parts following SLS and then sintered. Using parts containing spiral channels, a methodology was proposed that defines dimensionless parameters to describe channel dimensions that influence channel clearing. It was shown that this methodology provides accurate predictions for success in producing green parts while greatly minimizing the number of experiments compared to a traditional 4-variable design-of-experiment. The number of experiments required increases exponentially with the number of independent variables, so by dropping the number of variables from 4 to 2, the number of experiments can be reduced considerably. A dividing line can be determined for any design window using as few as 4 experiments (2 levels of testing for each variable) but more experiments are advantageous because the accuracy increases with the number of testing levels per variable. In addition to the dimensionless parameters that were utilized, it was found that the absolute value of the channel diameter is also important because there are diameters above which all channels were clearable (4.5 mm) and below which no channels were clearable (1.5 mm), independent of the values of scaled diameter and the tortuosity. These critical diameters are not intrinsic to the part geometry, but rather are related to the particle size used in the experiment. The nylon particles used in this study had a mean diameter of

55 µm so it stands to reason that a finer powder would allow smaller channel diameters to be cleared. However, this needs to be balanced against other considerations in the process. For SLS, powders that are much finer may be difficult to spread into layers and thus other failure mechanism may arise.

Another potential pitfall when producing glass or ceramic parts using indirect SLS is macroscopic distortions of the part geometry that can occur during debinding or sintering. The temperature profile during debinding must be selected to ensure that gas pressure from by-products of pyrolysis does not increase sufficiently in the part to cause it to distort or crack. In practice, this means that long debinding times may be required, especially for large parts that contain a low fraction of channels. The choice of sintering temperature is also important because if the sintering temperature is too low, the parts will not densify adequately and if it is set too high, the parts will deform due to viscous flow. It was demonstrated that though proper choices of the debinding temperature profile and the sintering temperature it is possible to produce parts that were free of gross distortions, even for samples with a very low pitch, long length, and small channel diameter which would be expected to be more susceptible to slumping or warping. Thus, with appropriate selection of powders, the debinding profile, and the sintering temperature, clearing of the powder out of the channels in the green parts is the largest hurdle with regards to producing a successful final part.

The x-ray tomographs and the density measurements performed using geometrical analysis both showed that the glass walls around the channels were not fully densified during sintering. The relative density of the walls compared to pure glass frit for these parts was ~62% with a standard deviation of +/- of 10.4%. This residual porosity resulted

primarily from the removal of the polymer particles which were much larger than the surrounding glass particles. Although higher sintering temperatures might increase the density of the walls somewhat, this would come at the expense of increased warping or slumping during sintering. A better approach would be to use an enhanced mixing method such as spray drying or thermally induced phase separation (TIPS). These methods would produce relatively homogenous mixtures of the polymer and ceramic that would improve the sinterability and increase final densities.

The parts made for this study were built horizontally rather than vertically within the powder bed. This likely lead to slightly oval channels rather than the desired circular channels. These channels were built in this orientation to reduce build time, but better geometric features could be achieved if the parts were built vertically. The choice of build orientation may influence design rules. For example, a vertically printed part may allow for a smaller channel diameter value that is still able to be cleared compared to the results of this study. Nevertheless, the methodology presented here could be repeated to produce new allowable design rules for the vertically built channels.

Chapter 3: Production of Optical Quality Parts to Influence Quantum Number

3.1: Orbital Angular Momentum in Optical Systems

Photons have spin angular momentum (represented by +/- h) and in some cases orbital angular momentum (represented by ℓ). The spin angular momentum of photons is related to their polarization. In paraxial optical systems such as fiber optics, this spin

angular momentum is in the direction of the propagation of the light. Orbital angular momentum on the other hand is not related to polarization but rather the phase of the light propagating through the medium (Bliokh [20]). As mentioned in the introduction, spiral phase plates and twisted fibers have been used to change the quantum number of photons by adding orbital angular momentum.

Spiral phase plates impart orbital angular momentum utilizing a material of refractive index n with a spiral-shaped thickness gradient around the central axis. Utilizing a focused beam and a small enough step size (the height between the highest and lowest point of the phase plate), the non-axial effects are minute enough to be considered negligent. In this fashion, the shift in the beam is considered to be in the phase only. (Beijersbergen *et al.* [17]).

Twisted fiber optic cables introduce a similar effect with spiraling channels that act as impellers throughout a fiber optic cable to create vortices of photons. Some benefits of this are that it can operate without a core and that the orbital angular momentum can be roughly maintained over long lengths of fiber optic cable (Russell *et al.* [18]). However, geometric distortion does occur as a result of twisting during the drawing process. Additionally, stress and strain introduced in the twisting and drawing process can drastically reduce the functionality of the fiber.

Taking these prior examples into consideration, a methodology was produced to additively manufacture a part that would similarly impact orbital angular momentum in a fiber optic system.

3.2: METHODS

In order to confirm optical properties necessary for use in a fiber optic application, flat sample bars were created using the powder mix and sintering specifications detailed previously. One side of the bar was left as-sintered and the other side was wet-sanded using SiC paper starting at a grit of 220 and then using successively finer grits up to 3000 grit to produce a flat and more reflective surface. Following the confirmation of these test bars for optical qualities, glass parts made via indirect selective laser sintering were produced to attempt to experimentally confirm that they could be used to apply orbital angular momentum to light passing through the helical channel.

3.3: RESULTS

In order to analyze the viability for optical manipulation, reflectivity measurements were taken for both sides over a wavelength range representing the UV/visible spectrum of approximately 200 to 1100 nanometers with a data point collected every 2 nanometers. These measurements were made at L3-Harris by members of their optical performance lab using general microscopy with a reflectivity fixture to analyze the reflectivity of the surfaces. The results can be seen in Fig. 13.

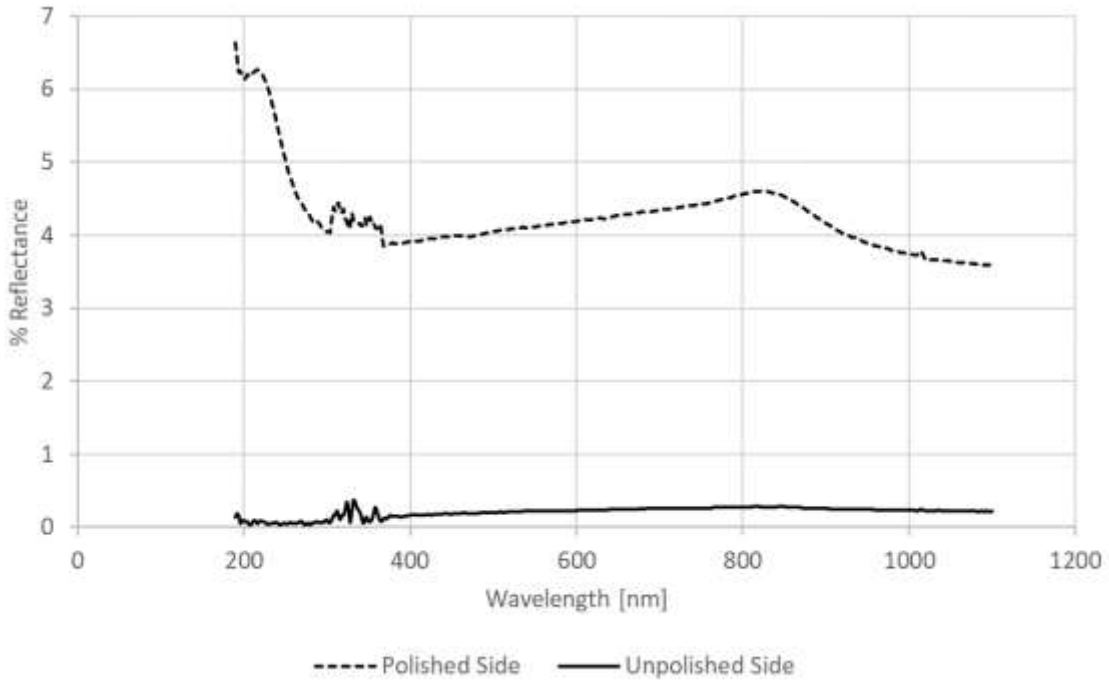

Figure 13. Reflectance of sample bar at various wavelengths

The reflectivity of the unpolished side was, as expected, very low (<<1%) because the surface roughness caused severe specular scattering of the light. The reflectivity of the polished side was quite a bit higher (3.5% -6.5%, depending on wavelength) than that of the unpolished side, but it was still quite low compared to optical quality glass. The low reflectivity indicates that there is scattering happening on a large scale across all wavelengths. However, this is to be expected given the relatively low densities discussed in Chapter 2. Increasing the density through methods such as TIPS or spray drying could result in much higher optical reflectance making the entire system more efficient.

Notably, the reflectance for the unpolished side remained relatively flat throughout the span of the wavelengths of interest. While the reflectivity itself is quite low compared

to the polished side, this consistency in the reflectivity with wavelength is optimal for optical applications in which light of various wavelengths may be used. For the purpose of demonstrating a proof-of-concept, increasing the intensity of the light entering the spiral would offset the effects of scattering. This would result in the necessary output for testing despite the low reflectivity so that the principle of quantum numbers changes using internal spiral geometries could be experimentally demonstrated.

Given the results of the preliminary optical testing on flat parts, test parts were designed utilizing the guidelines summarized in Chapter 2 such that they could add orbital angular momentum to a beam of light in order to increase the quantum number of the beam. A total of four geometries were created with the only variable between them being the helix diameter (D) such that the part could be made thinner in the event that debinding on a larger part became problematic. One difference between the model used in Chapter 2 compared to this one is the angle of the circular cross section used to create the channel. In Chapter 2, this circular channel cross section sat parallel to the top face of the cylinder meaning that any slice of the part taken perpendicular to the cylindrical axis would yield a slice with a circular hole. In the newly designed parts, the circle is orthogonal to the helix path at all points yielding an ellipse at each slice perpendicular to the cylindrical axis. This actually increases the channel area, meaning that the findings from Chapter 2 can be utilizes as conservative estimates. Additionally, the parts were built vertically within the powder bed to increase the resolution involved with forming the channels given that resolution in x and y is greater in most SLS systems than in z (into the powder bed). A representative part model can be seen in Fig. 14, and a table of dimensional values for the test parts can be seen in Table 4.

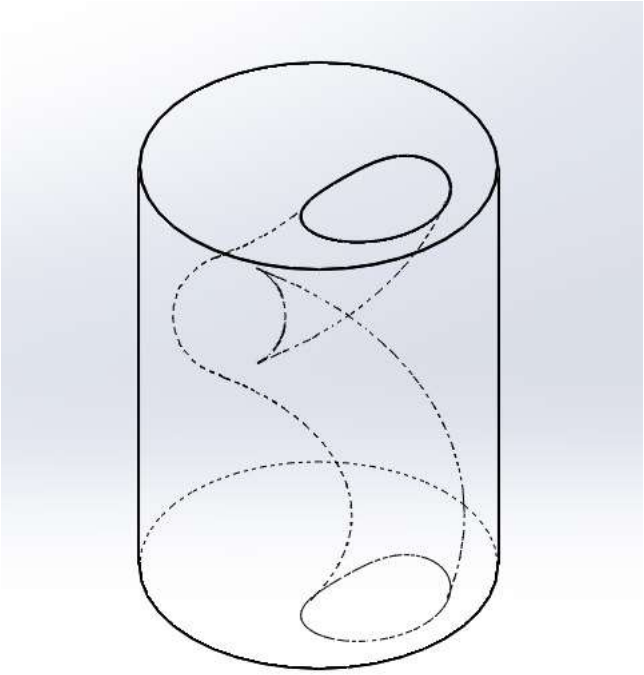

Figure 14. Representative part model

Part	d (mm)	p (mm)	L (mm)	D (mm)	Scaled Diameter	Tortuosity
1	4.5	19.05	19.05	5.08	0.236	3.75
2	4.5	19.05	19.05	5.715	0.236	3.33
3	4.5	19.05	19.05	6.35	0.236	3.00
4	4.5	19.05	19.05	6.985	0.236	2.73

Table 4. Helical part dimensions for optical testing

The geometrical parameters for each of these parts fell above the parting line established in Chapter 2, meaning the channels should be clearable using the methodology described. Additionally, a channel diameter of 4.5 mm (the diameter at which all samples produced clearable channels) was selected to ensure that the powder would flow smoothly out of the channels prior to debinding. As a result, the powder did flow out of the channels of the green parts quite easily (without requiring the use of compressed air to force out any stubborn remnants). Each green part had an aspect ratio between 1.041 and 1.061 indicating minor elongation in the y direction on the print bed. The parts were debinded following the procedure outlined in Fig. 6 and subsequently sintered at 575 °C. The sintered parts can be seen in Fig. 15. Despite efforts taken to mitigate warping during the debinding step by burying the sample in silica powder and covering the open face of the crucible, the parts show slight warpage on the upward facing surface as a result of convective cooling. This is seen as the slight right-facing bend on all four parts. These parts were then sent to L3-Harris for optical testing. The closure of laboratories across the country in March/April 2020 due to the Covid-19 pandemic slowed research progress significantly and prevented the tests from being conducted before this thesis was completed.

Figure 15. Sintered glass parts for optical manipulation

3.3: DISCUSSION

Parts were fabricated using indirect selective laser sintering for use as preforms within a fiber optic system in order to manipulate light utilizing internal helical channels to reflect incoming light beams. The goal of this is to produce orbital angular momentum, an additional degree of freedom for light beams which can take on theoretically limitless states, thus vastly increasing the bandwidth of information that can be transmitted via the light beam. Reflectance was measured for flat parts created using the same fabrication technique, and the results indicated that the optical properties of this particular material may be suitable. The geometries deemed capable of production in Chapter 2 introduce possibilities for end-use parts to accomplish this goal. Further testing and optimization is necessary to confirm this methodology as a suitable candidate to create orbital angular momentum.

Chapter 4: Conclusions and Future Work

4.1: Design Methodology

This study proposes a methodology for determining design rules for helical interior channels for parts made via selective laser sintering. For this project, a nylon/glass mix was used as the powder feedstock. It was found that the primary factor that controls whether a particular geometry can be successfully produced is the ability to clear loose powder from the channels in the green part. Dimensionless values of scaled diameter and tortuosity were defined from the four initial dimensional parameters (channel diameter, part length, helical pitch, and helical diameter) by considering the likely factors that influence the ability to clear loose powder from the green parts following SLS. It was demonstrated that this methodology simplifies the experimentation process and minimizes the number of tests required compared to conventional design of experiments. These dimensionless values can provide a reasonably accurate qualification of success for clearing the powder out of the channels. Two regimes separated by a line were obtained from this model that predict success and failure. Experiments showed that these regimes could be used to predict success with 93.3% accuracy and failure with 79.2% accuracy. More false-negatives than false-positives indicates that this model may be conservative in predicting channel clearing success. The design rules proposed in this research are powder-specific and machine-specific, but the methodology should prove viable for any powder mixture and SLS machine so long as that the mixture is suitable for sintering.

4.2: Parts for Optical Manipulation

The parts produced in this research are candidates to add orbital angular momentum to light beams through the use of precisely places internal helical channels. By varying the

geometric properties of the channels, different levels of orbital angular momentum may feasibly be reached. Since the variants of orbital angular momentum are theoretically limitless, achieving this change would represent the ability to greatly increase the bandwidth of data sent through optical systems while also having enormous implications in fields such as quantum computing and digital communication. Further testing is necessary to confirm or deny whether these parts have suitable geometries, densities, and inherent optical properties to successfully achieve this goal.

4.3: FUTURE WORK

Several approaches could be taken to improve the powder mixing technique in order to create denser parts which would yield better optical properties by reducing scattering. As mentioned previously, mixing methods such as thermally induced phase separation (TIPS) (Shahzad *et al.* [21]) or spray drying (Subramanian *et al.* [22]) would promote more homogeneous mixtures of polymer and glass particles that are more closely matched in size. The current mixing approach results in large polymer particles that leave large pores after pyrolysis that are difficult to sinter. A more homogenous mixture of smaller particles would eliminate these difficult-to-sinter pores. TIPS and spray drying approaches may also allow for a lower volume percent of polymer to be used while still successfully forming robust green parts through the SLS process, thus further increasing the relative density of the final parts. Finally, additional polymers or glasses could be selected to optimize optical properties for end-use parts. The materials selected for this research were chosen due to widespread availability and processing familiarity. The debinding conditions that were used were selected because they produced viable parts. However, additional optimization of the debinding and sintering processes could be

conducted to determine the true optimal ramp rates, temperatures, air flow rates. This would reduce the time to debind and sinter the parts and could result in parts that maintain better dimensional accuracy.

Additionally, for practical applications, finer feature resolution of both the helix and the glass parts are desired. To produce these fibers containing helical channels, the fiber preforms that were the focus of this thesis would need to be drawn or extruded. This could in principle be performed on the green parts before sintering and would also aide in debinding as it would decrease the diffusion distances for gasses during pyrolysis, which is one of the limiting factors in selecting debinding schedules for the larger preforms. It is likely that some additional experiments would be required to optimize the drawability of the fiber preforms.

Due to extenuating circumstances caused by the Covid-19 pandemic, optical testing could not be completed for the helical parts discussed in Chapter 3. For this reason, an obvious avenue of future work would be to demonstrate that the parts do adequately change the quantum number of light by introducing orbital angular momentum. Depending on these results, further design iterations could be produced to more readily achieve the desired result. After the successful completion of a part containing a single helical channel, the introduction of multiple channels, both separate and intertwining, could be introduced to further increase the bandwidth of the light traveling through the part.

Appendix

Part	d (mm)	p (mm)	L (mm)	D (mm)	Scaled Diameter	Tortuosity	Cleared?
1	4	38.1	25.4	4.50	0.157	8.47	Yes
2	3	20.0	25.4	4.50	0.118	4.44	No
3	3	38.1	25.4	4.50	0.118	8.47	No
4	4	38.1	15.0	4.50	0.267	8.47	Yes
5	4	38.1	25.4	2.00	0.157	19.05	Yes
6	3	30.0	15.0	6.00	0.200	5.00	Yes
7	3	30.0	38.1	2.00	0.079	15.00	No
8	4	30.0	38.1	2.00	0.105	15.00	Yes
9	3	30.0	38.1	3.00	0.079	10.00	No
10	3	50.0	10.0	4.00	0.300	12.50	Yes
11	3	14.0	15.8	5.60	0.190	2.50	No
12	3.5	12.0	20.6	4.80	0.170	2.50	No
13	3	30.0	17.6	6.00	0.170	5.00	Yes
14	2.5	25.0	16.7	5.00	0.150	5.00	No
15	4.5	40.0	30.0	5.33	0.150	7.50	Yes
16	3.5	20.0	26.9	2.67	0.130	7.50	Yes
17	2.5	41.0	19.2	4.10	0.130	10.00	yes
18	3	29.0	27.3	2.90	0.110	10.00	No
19	3.5	32.0	31.8	2.56	0.110	12.50	Yes
20	4.5	41.0	50.0	3.28	0.090	12.50	Yes
21	5	26.0	55.6	1.73	0.090	15.00	Yes
22	4	30.0	57.1	2.00	0.070	15.00	Yes
23	4.5	18.0	64.3	1.03	0.070	17.50	Yes
24	2.5	30.0	14.7	6.00	0.170	5.00	Yes
25	3.5	30.0	20.6	6.00	0.170	5.00	Yes
26	4.5	30.0	26.5	6.00	0.170	5.00	Yes
27	3.5	10.0	20.6	2.00	0.170	5.00	Yes
28	3.5	15.0	20.6	3.00	0.170	5.00	Yes
29	3.5	20.0	20.6	4.00	0.170	5.00	Yes
30	2.5	30.0	35.7	2.00	0.070	15.00	No
31	3.5	30.0	50.0	2.00	0.070	15.00	No
32	4.5	30.0	64.3	2.00	0.070	15.00	Yes
33	3.5	15.0	50.0	1.00	0.070	15.00	No
34	3.5	45.0	50.0	3.00	0.070	15.00	Yes
35	3.5	60.0	50.0	4.00	0.070	15.00	Yes

36	5	10.0	66.7	5.00	0.075	2.00	Yes
37	4.5	10.0	60.0	5.00	0.075	2.00	Yes
38	4	10.0	53.4	5.00	0.075	2.00	No
39	3.5	10.0	46.7	5.00	0.075	2.00	No
40	2	50.0	10.0	2.00	0.200	25.00	Yes
41	1.5	50.0	7.5	2.00	0.200	25.00	Yes
42	1	50.0	5.0	2.00	0.200	25.00	No
43	0.5	50.0	2.5	2.00	0.200	25.00	No
44	2.5	30.0	20.8	3.00	0.120	10.00	Yes
45	3	30.0	25.0	3.00	0.120	10.00	Broke
46	3.5	30.0	29.2	3.00	0.120	10.00	Broke
47	4	30.0	33.3	3.00	0.120	10.00	Yes
48	3.5	15.0	29.2	1.50	0.120	10.00	Yes
49	3.5	45.0	29.2	4.50	0.120	10.00	Yes
50	3.5	60.0	29.2	6.00	0.120	10.00	Yes
51	4.5	18.0	22.5	3.00	0.200	6.00	Yes
52	3.5	36.0	18.4	4.50	0.190	8.00	Yes
53	4.5	54.0	30.0	4.50	0.150	12.00	Yes
54	3.5	52.5	25.0	3.50	0.140	15.00	Yes
55	2.5	81.0	20.8	4.50	0.120	18.00	Yes
56	5	12.5	50.0	2.50	0.100	5.00	Yes
57	3	28.0	37.5	3.50	0.080	8.00	Yes
58	4.5	18.0	75.0	1.50	0.060	12.00	Yes
59	3	24.0	60.0	1.50	0.050	16.00	No
60	2.5	37.5	62.5	2.50	0.040	15.00	No
61	4.5	10.0	30.0	4.50	0.150	2.22	Yes
62	4.5	15.0	30.0	4.50	0.150	3.33	Yes
63	4.5	20.0	30.0	4.50	0.150	4.44	Yes

Table 5. Helix dimensions

References

[1] Klein, John & Stern, Michael & Franchin, Giorgia & Kayser, Markus & Inamura, Chikara & Dave, Shreya & Weaver, James & Houk, Peter & Colombo, Paolo & Yang, Maria & Oxman, Neri. (2015). Additive Manufacturing of Optically Transparent Glass. 3D Printing and Additive Manufacturing. 2. 10.1089/3dp.2015.0021.

[2] Zocca, Andrea & Colombo, Paolo & Wirth (Cynthia M. Gomes), Cynthia & Günster, Jens. (2015). Additive Manufacturing of Ceramics: Issues, Potentialities, and Opportunities. Journal of the American Ceramic Society. 98. 10.1111/jace.13700.

[3] J. Allison, C. Sharpe, and C. C. Seepersad, "A Test Part for Evaluating the Accuracy and Resolution of a Polymer Powder Bed Fusion Process," J. Mech. Des., vol. 139, no. 10, p. 100902, Aug. 2017, doi: 10.1115/1.4037303.

[4] J. Allison, C. Sharpe, C. C. Seepersad, and S. Kubiak, "POWDER BED FUSION METROLOGY FOR ADDITIVE MANUFACTURING DESIGN GUIDANCE," p. 20.

[5] "Design Guidelines – Design for AM Knowledge Base." [Online]. Available: http://designforam.me.utexas.edu/polymer-pbf/design-rules-2. [Accessed: 07-Jan-2020].

[6] Adam, G. and Zimmer, D. (2015), "On design for additive manufacturing: evaluating geometrical limitations", Rapid Prototyping Journal, Vol. 21 No. 6, pp. 662-670. https://doi.org/10.1108/RPJ-06-2013-0060

[7] L. Milisits, "Methodology for Mechanical Property Optimization of Selective Laser Sintered Parts Using Design of Experiments," Thesis, University of Texas at Austin, Austin, 2017.

[8] A. Thompson, "Surface texture measurement of metal additively manufactured parts by X-ray computed tomography," p. 292.

[9] Deckers, J., Shahzad, K., Cardon, L., Rombouts, M., Vleugels, J. and Kruth, J. (2016), "Shaping ceramics through indirect selective laser sintering", Rapid Prototyping Journal, Vol. 22 No. 3, pp. 544-558. https://doi.org/10.1108/RPJ-10-2014-0143

[10] Xiao K, Dalgarno KW, Wood DJ, Goodridge RD, Ohtsuki C (2008) Indirect selective laser sintering of apatite-wollostonite glass-ceramic. Proc Inst Mech Eng H 222(7):1107–1114

[11] K. Shahzad, J. Deckers, J.P. Kruth, J. Vleugels, Additive manufacturing of aluminaparts by indirect selective laser sintering and post processing, J. Mater. Process.Technol. 213 (9) (2013) 1484–1494.

[12] Wang, J., Yang, J., Fazal, I. et al. Terabit free-space data transmission employing orbital angular momentum multiplexing. Nature Photon 6, 488–496 (2012). https://doi.org/10.1038/nphoton.2012.138
[13] Zhao, Yunhe & Wang, Tianxing & Mou, Chengbo & Yan, Zhijun & Liu, Yunqi & Wanga, Tingyun. (2018). All-Fiber Vortex Laser Generated With Few-Mode Long-Period Gratings. IEEE Photonics Technology Letters. PP. 1-1. 10.1109/LPT.2018.2815041.
[14] Keck, D. B., & Schultz, P. C. (1970). U.S. Patent No. US3711262A. Washington, DC: U.S. Patent and Trademark Office.
[15] Yeh, C. (1990). The Optical Fibers: Fiber Fabrication. In *Handbook of fiber optics: Theory and applications* (pp. 24-26). San Diego, CA: Academic Press.
[16] Massari, Michele & Ruffato, Gianluca & Gintoli, Michele & Ricci, Francesco & Romanato, Filippo. (2015). Fabrication and characterization of high-quality spiral phase plates for optical applications. Applied Optics. 54. 10.1364/AO.54.004077.
[17] Beijersbergen, Marco & Coerwinkel, R.P.C. & Kristensen, M. & Woerdman, J.P.. (2016). Helical-wavefront laser beams produced with a spiral phaseplate.
[18] Russell, P. & Beravat, Ramin & Wong, G.. (2017). Helically twisted photonic crystal fibres. Philosophical Transactions of The Royal Society A Mathematical Physical and Engineering Sciences. 375. 20150440. 10.1098/rsta.2015.0440.
[19] Fluegel, A. (2007), Global Model for Calculating Room-Temperature Glass Density from the Composition. Journal of the American Ceramic Society, 90: 2622-2625. doi:10.1111/j.1551-2916.2007.01751.x
[20] Bliokh, Konstantin & Nori, Franco. (2015). Transverse and longitudinal angular momenta of light. Physics Reports. 592. 10.1016/j.physrep.2015.06.003.
[21] Shahzad, Khuram & Deckers, Jan & Zhang, Zhongying & Kruth, Jean-Pierre & Vleugels, Jef. (2014). Additive manufacturing of zirconia parts by indirect selective laser sintering. Journal of the European Ceramic Society. 34. 81-89. 10.1016/j.jeurceramsoc.2013.07.023.
[22] Subramanian K, Zong G, Vail N, Barlow J, Marcus H, (1993) Selective laser sintering of Al_2O_3, Proc. 4^{th} Solid Freeform:350

Vita

Permanent email: Joe.Nissen94@gmail.com

This thesis was typed by Joseph Michael Nissen.